The Astronomical Journal, 135:55–67, 2008 January doi:10.1088/0004-6256/135/1/55

NEAR-INFRARED SPECTRA OF CENTAURS AND KUIPER BELT OBJECTS

K. M. Barkume, M. E. Brown, and E. L. Schaller
Division of Geological and Planetary Sciences, California Institute of Technology, Pasadena, CA 91101, USA; barkume@caltech.edu
Received 2007 July 13; accepted 2007 August 26; published 2007 November 29

ABSTRACT

We present here an extensive survey of near-infrared (NIR) spectra of Kuiper belt objects (KBOs) and Centaurs taken with the Keck I Telescope. We find that most spectra in our sample are well characterized by a combination of water ice and a featureless continuum. A comparative analysis reveals that the NIR spectral properties have little correlation to the visible colors or albedo, with the exception of the fragment KBOs produced from the giant impact on 2003 EL61. The results suggest that the surface composition of KBOs is heterogeneous, though the exposure of water ice may be controlled by geophysical processes. The Centaurs also display diverse spectral properties, but the source of the variability remains unclear. The results for both the KBOs and the Centaurs point to inherent heterogeneity in either the processes acting on these objects or materials from which they formed.

Key words: infrared: solar system – Kuiper Belt – minor planets, asteroids

Online-only material: supplemental data file

1. INTRODUCTION

The Kuiper belt poses a unique opportunity for astronomers to peer back into the formation of our solar system. Composed of the debris left after planet formation, Kuiper belt objects (KBOs) are thought to be among the most pristine bodies in the solar system. However, KBOs have likely undergone some alteration since their formation from geophysical, collisional, and space weathering processes. Centaurs may have undergone even more alteration as their temperatures are increased by closer perihelion passages. KBOs span several orders of magnitude in diameter, and at small sizes they are thought to resemble comets and be composed largely of primordial materials that remained at relatively low temperatures. The largest members of the Kuiper belt, such as Eris and Pluto, resemble planets with tenuous atmospheres, active resurfacing, and possibly differentiated interiors. While this size spectrum provides a singular opportunity to study a variety of planetary processes, the largest objects may be very different from their smaller brethren. This complicates the task of understanding the small bodies by extrapolating results from the more easily studied large objects. Furthermore, the surfaces of all these objects are also likely to be altered by cosmic rays, impacts, and interstellar dust, thereby obscuring the materials from which they are made. Despite these complications, the study of KBOs will provide important clues to the formation of our solar system and the processes that continue to shape it.

Much effort has been put forth in the past decade to understanding the physical and chemical states of KBOs and Centaurs and is well summarized by Barucci et al. (2007). To date, over a hundred objects have measured photometric colors in visible wavelengths, but far fewer objects have spectra due to the faintness of KBOs. Spectra in the visible wavelengths are often characterized by a red continuum component typically identified as carbon-rich material and some objects may have subtle silicate spectral features. Near-infrared (NIR) spectra taken over the past decade have revealed a variety of ices on the surfaces of KBOs including methane, water, methanol, and nitrogen. Previous studies have shown that the largest KBOs, Eris, Pluto, and 2005 FY9 have spectra dominated by methane (see Barucci et al. (2007) and references therein). In the case of Pluto, N_2 and CO have also been detected. The presence of these species on the largest objects is likely due to their large masses which allow for volatiles to be retained (Schaller & Brown 2007). It has been noted that moderately sized KBOs, such as Quaoar and Orcus, often have surfaces dominated by water ice. Finally, the smallest KBOs and Centaurs for which we have spectra typically appear to be largely featureless in the NIR. The exception is a handful of smaller KBOs that have among the deepest water ice absorption features ever detected in the Kuiper belt. These objects have been shown to be dynamically associated with the large KBO 2003 EL61 and are thought to be fragments from its mantle that were ejected during a catastrophic impact (Brown et al. 2007b).

To date, there is no widely accepted standard model of KBO surface processes that accounts for the varying presence of water ice on the moderate to smaller KBOs. One commonly proposed model describes essentially a two-component surface made of dark, carbon-rich deposits and exposed, fresh water ice (Luu & Jewitt 1996). The dark surfaces are thought to be similar to those observed on comets or Saturn's moon, Phoebe, and are likely a mixture of materials (Clark et al. 2005). The spectral properties of the crusts are often characterized by amorphous silicate material, and irradiated, polymerized hydrocarbons called tholins (Moore et al. 1983), producing the red visible colors observed and nearly featureless spectra on most KBOs. In this model, fresh ice initially exposed by erosion, impact gardening, outgassing, or cryovolcanism creates a surface with strong water ice signatures. Over time, the surface eventually darkens and reddens as it becomes irradiated and a new crust forms, obscuring the water ice signatures.

Thus far most spectra have been analyzed individually offering only vignettes of KBO surface characteristics. A comparative study using the visible and NIR photometric colors of KBOs by Barucci et al. (2005) found four different color groups, though it remains unclear how these color groups relate to specific spectroscopic features or surface characteristics. Here we present a survey of low-resolution NIR spectra of bright KBOs and Centaurs taken with the near-infrared camera (NIRC) on the Keck I Telescope (Matthews & Soifer 1994). The uniformity of this survey allows us to study these objects comparatively as well as individually. Several of the objects in our survey that

showed evidence of particularly interesting or unique surfaces have already been published previously (e.g., 2005 FY9 and 2003 EL61). Thus, we concentrate here on a comparative study with the aim of understanding the surface processes that may be generally acting on the Centaur and KBO populations. We begin by describing our sample of observed objects in Section 2. We discuss the observations and data reduction in Section 3, and the analysis of the spectra, including the spectral fitting, in Section 4. We find that the properties of the collisional family members of 2003 EL61 differ from the general population of KBOs and therefore we describe our results for these two populations separately in Sections 5.1 and 5.2. Finally, we discuss impact that the results of this work have on our general understanding of the physical processes that occur in the outer solar system in Section 6.

2. THE SAMPLE

For our survey we preferentially selected KBOs with an absolute magnitude less than 5.0, corresponding to objects with a diameter longer than about ∼400 km, assuming a 10% albedo (Stansberry et al. 2007), though six KBOs have absolute magnitudes greater than 5.0. We excluded any KBOs and Centaurs with visual magnitudes greater than ∼21, which we found was our effective magnitude limit with NIRC. Targets located near the galactic plane were also abandoned due to contamination from field stars. Of the possible targets, the KBOs were evenly distributed between hot classical and resonant population, with a few objects belonging to the scattered disk. For the purpose of our survey, Centaurs are defined to be objects with perihelia less than 25 AU. No cold classical objects were observed due to the lack of bright targets in this population. In total, we observed 33 bright KBOs and 12 Centaurs with NIRC from 1998 March to 2007 April.

3. OBSERVATIONS AND DATA REDUCTION

Low-resolution ($\lambda/\Delta\lambda \sim 160$) spectra from 1.4 to 2.5 μm were obtained with NIRC for each object using a 150 lines μm^{-1} grism and an H–K-order sorting filter. A complete list of observations is provided in Table 1. Targets were identified in fields by their motion and tracked during observations by the telescope. The exposure times for the spectra were between 150 s and 300 s, but were typically 200 s. Dithering between subsequent images by 5 arcsec was used to subtract most of the background sky emission. Solar-type stars were observed for calibration purposes at similar air masses and times to target observations, with the typical differences in air mass being less than 0.1.

The raw image processing and spectral extraction were done using standard procedures. We first subtracted sequential images to remove most of the sky background emission and divided by a flat-field image constructed from a median dome flat. We then measured and removed any curvatures in the sky lines in individual images. Residual sky emission was measured on either side of the target spectrum and subtracted from the image. The spectrum was then extracted by summing in the spatial direction, typically a 7–10 pixel swath, centered on the target at each spectral position. Bad pixels were identified by visual inspection and removed. Spectra of calibration stars were extracted similarly with the exception of removing the curvature. Since exposures were too short for calibration sources to measure the skyline curvature accurately, the curvature measurements were used from target observations. Target spectra were then divided by a calibration star spectra taken at a similar air mass and time to remove atmospheric absorptions and produce a reflectance spectrum. A more detailed discussion of our data reduction methods is available in Brown (2000).

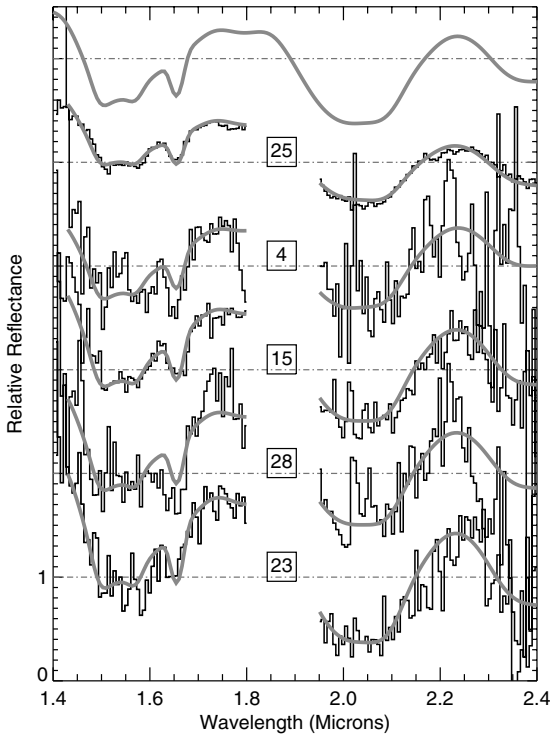

Figure 1. The relative reflectance spectra of 2003 EL61 and its collisional family. The KBOs shown above are 25: 2003 EL61, 4: 1995 SM55, 15: 2003 TX300, 28: 2005 RR43, and 23: 2003 OP32. Each spectrum is normalized to 1.0 (the dashed gray lines) and offset to allow for comparison. A model spectrum of pure water ice is also shown at the top (thick dark gray line). The region between 1.8 and 1.9 μm is masked due to the large errors introduced by H_2O telluric lines. The thick gray line represents the best-fit model to each spectrum and is a combination of water ice and a sloped continuum component. See Section 4 for more information on the modeling and Table 2 for the fit results.

The signal to noise was low in individual spectra and therefore multiple spectra were added together to obtain higher signal to noise. In many cases, spectra were added over multiple nights (see Table 1). Multiple spectra of a single target were then summed together weighted by their noise to produce a final spectrum. We examined individual spectra to look for substantial variability with time or rotational phase. We did not detect any significant variation in the spectra of any object, though small changes are undetectable due to noise. As such, the spectra we show here represent an average spectrum. High signal-to-noise spectra were obtained for most objects with an average of 6000 s of total integration time.

4. ANALYSIS

The reflectance spectrum for each object is shown in Figures 1–7. We broadly find that our results fit with the spectral trends seen previously for KBOs (see Barucci et al. (2007) for a review). The largest object in our survey, 2005 FY9, has spectral features dominated by methane ice, which has previously been explained by the low escape rate of volatiles on large KBOs (Schaller & Brown 2007). The lack of observed methane on the remaining objects in the sample supports the models of Schaller

Table 1
Journal of Observations

Number	Object	UT Date	Exposure Time (s)	Air mass	Calibration Source
		Kuiper belt objects			
1	15875 (1996 TP66)	2000 Jul. 22	5000	1.27–1.02	BD +17 209
		2000 Aug. 5	6200	1.21–1.02	BD +05 5212
		2000 Aug. 6	1000	1.01–1.02	BD +05 5212
2	19521 Chaos (1998 WH24)	2000 Sept. 15	11000	1.00–1.36	HD30701, SAO 149875
3	20000 Varuna (2000 WR106)	2001 Mar. 10	6000	1.47–1.05	HD 42112, HD 41919
					HD 42358, HD41880
4	24835 (1995 SM55)[a]	2006 Oct. 9	3000	1.10–1.20	HD 254985
5	26181 (1996 GQ21)	2001 Mar. 10	8000	1.14–1.38	HD 150583, HD 148592
					HD 151786, HD 149826
		2001 May 5	4000	1.14–1.27	HD 133688
6	26375 (1999 DE9)	2000 Mar. 10	6000	1.05–1.22	HD 43515, HD 40977
					HD 42112, HD 148116
7	28978 Ixion (2001 KX76)	2002 May 27	4000	1.29–1.39	HD100803
8	33340 (1998 VG44)	2003 Nov. 13	4000	1.00–1.03	HD 285216
9	38628 Huya (2000 EB173)	2000 Jun. 18	1800	. . .[b]	SAO 11973
		2000 Jun. 19	2700	. . .[b]	SAO 11973
10	42301 (2001 UR163)	2004 Nov. 22	3000	1.02–1.08	BD +09 93
11	47171 (1999 TC36)	2000 Aug. 6	5200	1.18–1.46	BD +05 5212
		2003 Nov. 11	4000	1.11–1.16	BD +07 173
12	47932 (2000 GN171)	2001 May 6	6000	1.10–1.18	HD 133688
13	50000 Quaoar (2002LM60)	2003 May 10	3000	1.22	HD 155731
		2003 May 12	7000	1.23–1.41	HD 161788, HD 155731
14	55565 (2002 AW197)	2003 Nov. 10	3000	1.02–1.04	HD 262124
		2003 Nov. 11	1000	1.07–1.10	BD +09 2095
		2003 Nov. 12	1000	1.14	BD +09 2095
15	55636 (2002 TX300)[a]	2003 Nov. 10	2000	1.01–1.00	HD 461
		2004 Sep. 5	5000	1.01–1.13	HD 4820
16	55637 (2002 UX25)	2003 Nov. 10	6000	1.01–1.04	HD 461, BD +07 369
17	55638 (2002 VE95)	2003 Nov. 11	8000	1.01–1.09	BD +8 615
18	66652 (1999 RZ253)	2000 Aug. 5	2000	1.33–1.23	HD 204741
		2000 Aug. 6	4000	1.22–1.43	HD 204741, BD +05 5212
19	84522 (2002 TC302)	2003 Nov. 13	5000	1.24–1.00	HD13650
20	84922 (2003 VS2)	2005 Oct. 15	4000	1.20–1.49	HD 281368
21	119951 (2002 KX14)	2003 May 10	3000	1.29–1.33	HD 143955
22	120132 (2003 FY128)	2003 May 5	3000	1.09–1.10	HD 113254
23	120178 (2003 OP32)[a]	2005 Oct. 15	4000	1.11–1.36	HD 206938
24	120348 (2004 TY364)	2005 Oct. 15	5000	1.18–1.25	HD 15907
25	136108 (2003 EL61)[a]	2005 Apr. 26	5000	1.01–1.19	HD 126694
26	136472 (2005 FY9)	2005 Apr. 26	3000	1.02–1.11	HD 113338
		2005 Apr. 27	6000	1.17–1.04	HD 100796
27	145452 (2005 RN43)	2006 Oct. 7	4000	1.07–1.08	HD 206938
28	145453 (2005 RR43)[a]	2006 Oct. 8	3000	1.05–1.15	G32–8
		2006 Oct. 9	3000	1.17–1.29	HD 34828
29	2003 AZ84	2004 Nov. 22	4000	1.01–1.12	HD 264528
					HD 63690
		2007 Apr. 5	5000	1.02–1.49	BD +13 1721, HD 77708
					BD +25 1858, HD 87860
		2007 Apr. 6	4000	1.02–1.10	HD 77708
30	2004 NT33	2005 Oct. 14	3000	1.06–1.01	BD +12 4466
31	2004 PG115	2004 Sep. 5	6000	1.08–1.23	SAO 144860
32	2005 QU182	2006 Oct. 9	4000	1.23–1.39	G 32–8
33	2005 UQ513	2006 Oct. 7	3000	1.07–1.09	BD +03 351
		2006 Oct. 8	3000	1.04–1.11	BD +14 4758
		Centaurs			
34	2060 Chiron (1977 UB)	1998 Aug. 03	500	1.76–1.83	SAO 159027 (A0)
35	5145 Pholus (1992 AD)	1998 Mar. 08	2000	1.05–1.22	SAO 100913 (A3)
36	8405 Asbolus (1995 GO)	1998 Mar. 07	1000	1.33–1.34	SAO 182160 (A2)
37	10199 Chariklo (1997 CU26)	1998 Mar. 07	1000	1.03–1.05	SAO 098558 (A2)
38	29981(1999 TD10)	2000 Aug. 6	4000	1.05–1.08	BD +05 5212
39	31824 Elatus (1999 UG5)[b]	. . .	. . .	. . .	. . .
40	52872 Okyrhoe (1998 SG35)	2003 Nov. 12	4000	1.04–1.08	HD 26064
41	54598 Bienor (2000 QC243)	2003 Nov. 11	6000	1.10–1.18	SAO 146792
					HD221221

Table 1
(Continued)

Number	Object	UT Date	Exposure Time (s)	Air mass	Calibration Source
42	65489 Ceto (2003 FX128)	2003 May 11	1800	1.05–1.41	HD160805, HD 107514
		2003 May 12	3200	1.04–1.07	HD 113254
		2007 Apr. 5	4000	1.25–1.65	BD +01 2956, HD 146396 HD 159741, HD 155598
		2007 Apr. 6	6000	1.05–1.25	HD 130875, HD 155598
43	83982 Crantor (2002 GO9)	2003 May 12	3000	1.07–1.13	HD 126170
44	95626 (2002 GZ32)	2003 May 11	2600	1.01	HD 107514
45	127546 (2002 XU93)	2003 Nov. 10	7000	1.03–1.17	HD 262124
		2003 Nov. 11	4000	1.01–1.03	HD 262125

Notes.
[a] 2003 EL61 and its associated family members.
[b] Observing log records could not be recovered.

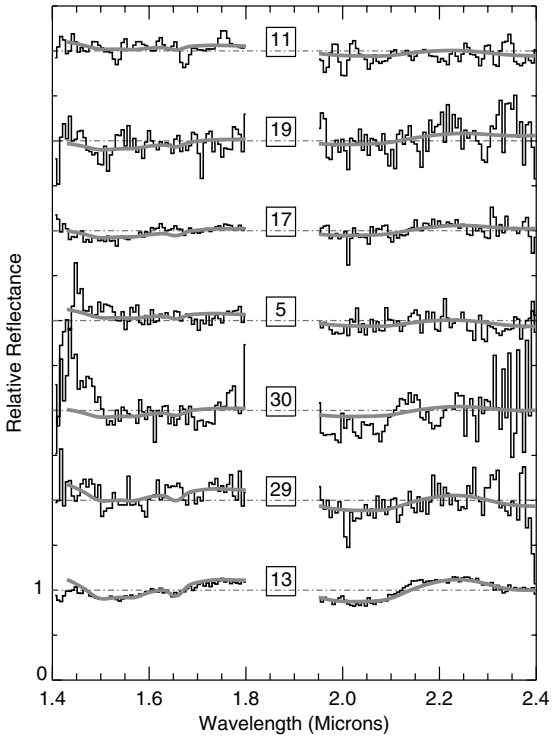

Figure 2. The relative reflectance spectra for the following KBOs—13: Quaoar, and 29: 2003 AZ84, 30: K40713A, 5: 1996 GQ21, 17: 2002 VE95, 19: 2002 TC302, and 11: 1999 TC36. The spectra are shown in decreasing fraction of water ice from bottom to top. See Table 2 for the fraction of water ice detected in the spectrum and the other fit results for the spectral models. Water ice is detected on Quaoar, 2003 AZ84, 1996 GQ21, 2002 VE95, and 1999 TC36 at the 3σ level or higher. 2002 TC302 has a 2σ detection of water ice. We do not detect additional ice species in the spectra of these KBOs.

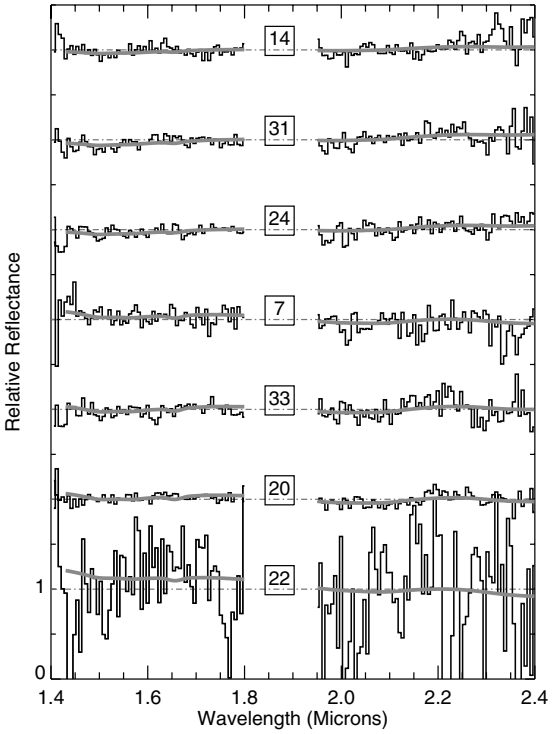

Figure 3. The relative reflectance spectra for the following KBOs—22: 2003 FY128, 20: 2003 VS2, 33: K51024A, 7: Ixion, 24: 2004 TY364, 31: K40804A, and 14: 2002 AW97. The spectra are shown in decreasing fraction of water ice from bottom to top. See Table 2 for the fraction of water ice detected in the spectrum and the other fit results for the spectral models. Water ice is detected on 2003 VS2 at higher than the 3σ level. It is marginally detected on K51024A, Ixion, 2004 TY364, and K40804 at least the 1σ level.

& Brown (2007), which suggests that differential loss rates of volatiles can provide a first-order explanation for the surfaces of KBOs and Centaurs. 2005 FY9 has been discussed in previous studies (e.g., Licandro et al. 2006; Brown et al. 2007a) and therefore will not be considered for further analysis.

With few exceptions, the remaining objects have either spectral signatures of water ice at 1.5 μm and 2.0 μm with varying line strengths or show no identifiable spectral features. Ideally, these spectra can provide information about the abundance of surface constituents. Approximations to the equations of radiative transfer for particulate surfaces have been developed by Hapke and others. They allow for the abundances and relative grain sizes of particles to be determined quantitatively using the reflectance spectra (Hapke 1993). However, in practice, it is difficult to obtain accurate abundances because of the uncertainties in a number of parameters. To begin, the true geometric albedo, not the relative reflectance, is needed to estimate abundances accurately and few objects in our survey have albedo measurements. For those with albedo measurements, uncertainties remain due to the limited knowledge of the particle scattering properties, degeneracies between intimate and geographic mixtures of the constituents, and poor constraints on the optical constants of the materials. With these difficulties in mind, we do not attempt to make precise surface models of the KBO in our survey. Still much can be learned by parameterizing the spectra of the whole population and comparing the relative strengths of

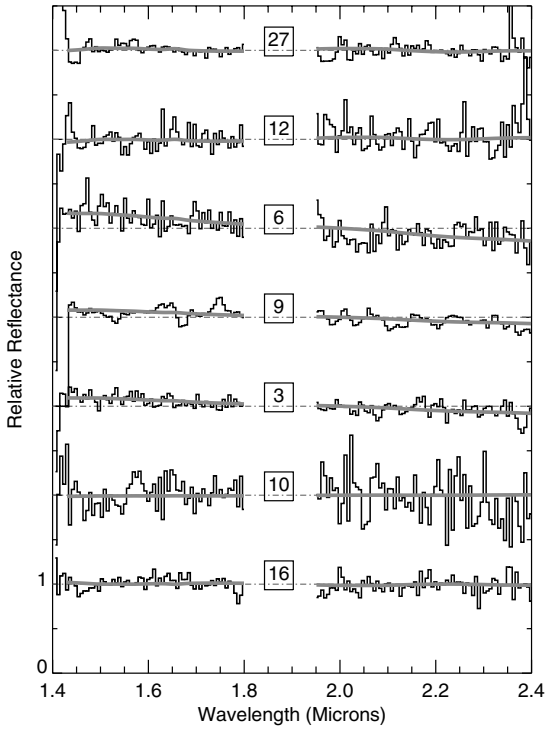

Figure 4. The relative reflectance spectra for the following KBOs—16: 2002 UX25, 10: 2001 UR163, 3: Varuna, 9: Huya, 6: 1999 DE9, 12: 2000 GN171, and 27: 2005RN43. The spectra are shown in decreasing fraction of water ice from bottom to top. See Table 2 for the fraction of water ice detected in the spectrum and the other fit results for the spectral models. No ices are detected on these KBOs.

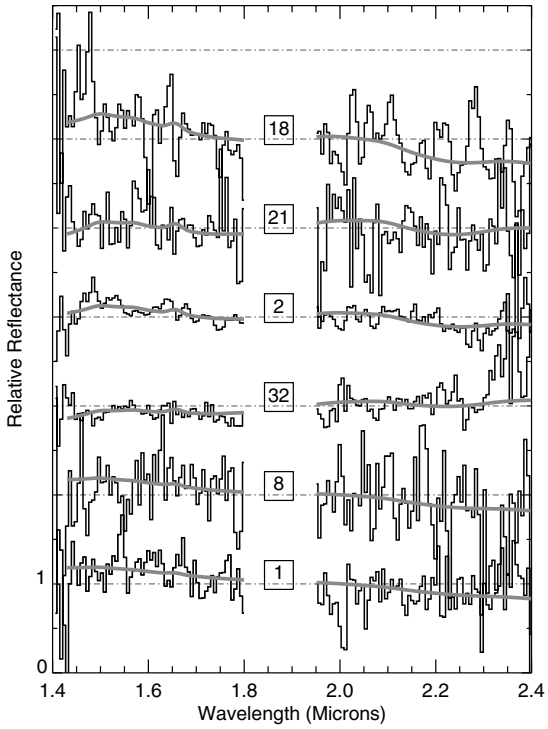

Figure 5. The relative reflectance spectra for the following KBOs—1: 1996 TP66, 8: 1998 VG44, 33: K50830B, 2: Chaos, 21: 2002 KX14, and 18: 1999 RZ256. The spectra are shown in decreasing fraction of water ice from bottom to top. See Table 2 for the fraction of water ice detected in the spectrum and the other fit results for the spectral models. Best-fit models produce negative f values for these KBOs which may be related to variable weather conditions during observation. See Section 5 for more details.

the spectral signatures of water ice on the surface using Hapke models. In particular, we can determine if the data are consistent with the simple two-component surface hypothesis of water ice and dark, carbon-rich material for the population as a whole. Furthermore, we can relate the fitted parameters of the spectra to other physical and chemical properties of the sample with the aim of determining the processes that control surface characteristics.

Previously, the spectra obtained in our survey were parameterized by finding the flux ratio between 1.7 μm region where water ice produces little absorption and the 2.0 μm region, which is at the bottom of the water ice absorption feature (Brown et al. 2007b). This method introduces large errors into the parameterization as only small portions of the spectrum are utilized. To use the full information available in our spectra, we create spectral models of the surface reflectance between 1.4 and 2.4 μm using the equations of radiative transfer developed by Hapke (1993). To allow for comparison between objects, each spectrum was normalized to 1.0 by finding the median reflectance between 1.4 and 2.5 μm. The region near the 1.8 μm telluric water lines was excluded due to the large errors in this wavelength region. After each spectrum was normalized, it was fit with a spectral model using a least-squares minimization scheme that utilizes the Powell method for finding minima. A linear reflectance model of water ice and a continuum component was fit to each spectrum and solved for f, the fraction of water in the spectrum, and m, the slope of the continuum component. The model can be written as

$$R(f, m, \lambda) = f\mathcal{R}_w(T, g, \lambda) + (1 - f)(m(\lambda - 2.0\,\mu\text{m}) + 1.0)). \quad (1)$$

$\mathcal{R}_w$ is the reflectance spectrum of water ice calculated using the optical constants from Grundy & Schmitt (1998) at temperature, T, and for grain size, g. The spectral features of water ice show only slight changes with temperatures in the range expected for the Kuiper belt, and therefore the temperature was set to 50 K (Grundy & Schmitt 1998). The grain size, which parameterizes the optical path length through the ice, affects both the line shape and depth of water ice absorption features but has been found to be between ~20 and ~100 μm on KBOs. To allow f to be compared across all objects, we set the grain size to 50 μm, though different grains may exist on some objects. The slope of the continuum component, m, is allowed to vary but the reflectance of the continuum is constrained to be 1.0 at 2.0 μm. To match the model to the data, we normalize the model using the same method of dividing by the median that was used to normalize the data. The error in the reflectance at each wavelength used to calculate χ^2 was found by first subtracting a smoothed spectrum from the data and finding the standard deviation of the surrounding pixels. The smoothed spectrum was created using a boxcar average of a 9 pixel wide region centered at each wavelength and the standard deviation was calculated over the same 9 pixel swath.

Formal statistical 1σ errors in the fit parameters were found by determining the values of f and m that produced χ^2 values equal to $\chi^2_{\text{min}} + 1$, where χ^2_{min} is the minimum χ^2 value (Bevington & Robinson 1993). However, the formal statistical errors do not take into account systematic errors and we find that they likely underestimate the true errors in our data. To obtain better estimates of the true errors, we selected objects in our survey whose spectra appeared to be consistent with no water

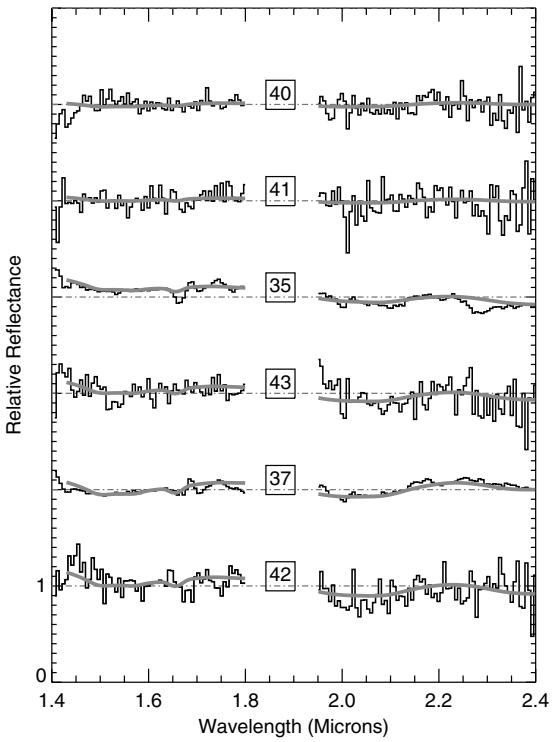

Figure 6. The relative reflectance spectra for the following Centaurs—42: Crantor, 37: Chariklo, 35: Pholus, 43: Ceto, 41: Bienor, and 40: Okyrhoe. The spectra are shown in decreasing fraction of water ice from bottom to top. Water ice is detected on Crantor, Chariklo, Pholus, and Ceto at the 3σ level or higher. Bienor and Okyrhoe have detections of water ice at a level between 1σ and 3σ. See Table 2 for the fraction of water ice detected in the spectrum and the other fit results for the spectral models.

ice by visual inspection. For these objects, we determined the actual error required to have an f consistent with 0 within 3σ errors. We found that the formal statistical errors underestimated the true errors by a factor of $\sim$2 for these objects and therefore we take the actual 1σ errors to be twice what was found by the formal statistics for all objects. The fit parameters for each object are listed in Table 2.

In addition to the spectral parameters we measured from the NIR spectra, we considered the visible color gradients of the objects, which are thought to be diagnostic of the carbon-rich materials on KBOs. It has been shown that the visible spectrum of KBOs between 0.5 μm and 0.8 μm is well described by a single color gradient, G_v, measured using broadband photometry (Hainaut & Delsanti 2002). We obtained visible color measurements for 35 of the 45 objects in our survey from published sources (see Table 2 for the full list) and calculated the color gradient and its uncertainty using the V, R, and I colors and the method described in Hainaut & Delsanti (2002). Five objects had no I-band measurements and one object had no R-band measurement. The spectral gradients were calculated for these objects using only the two available measurements. We find that the average difference in the gradient calculated using two versus three reflectance measurements is small compared to the errors in the color measurements. We also consider the sizes, albedos, and orbital characteristics of those objects in our survey for which measurements are available to gain a comprehensive understanding of these objects. The sizes and albedos are taken from Stansberry et al. (2007) and are reproduced in Table 3 along with the orbital elements of the objects in our survey.

5. RESULTS

We find that most of the spectra are well fitted by our two-component model and that the spectra had a final reduced $\chi^2_{\rm min}$ of $\sim$1. See Figures 1–7 for the spectra and the best-fit models. Other than 2005 FY9, we find no compelling detections of additional ices such as NH_3, CH_4, CO, or CO_2, which are observed on some outer solar system bodies, though these species may be present in low abundances. Detections of NH_3 have been reported for Charon and Quaoar (Brown & Calvin 2000; Jewitt & Luu 2004). Our spectrum of Quaoar shows a similar flattening at 2.2 μm that was observed by Jewitt & Luu (2004) but $\chi^2_{\rm min}$ is not significantly decreased by the inclusion of NH_3 or its hydrate. CH_3OH has been previously detected on Pholus and 2002 VE95 (Cruikshank et al. 1998; Barucci et al. 2006). We find that our two-component model works poorly for Pholus unless the region near the 2.3 CH_3OH absorption line is excluded. A three-component model that included CH_3OH was constructed to determine if a better fit could be made by including this ice. We find that Pholus had a significant decrease in the $\chi^2_{\rm min}$ value by including CH_3OH. For 2002 VE95, we find that the inclusion of CH_3OH did not produce a significantly better fit to our spectrum and that our measured fraction of CH_3OH in the spectrum is consistent with 0. However, up to 25% of the surface can be CH_3OH without being detected in our spectrum due to the lower signal to noise beyond 2.2 μm. Consequently, our spectrum may have insufficient signal to noise to detect the feature seen by Barucci et al. (2006). We find that 1996 GQ21, which has similar spectral features to Pholus, also does not have a significant detection of CH_3OH, but the signal to noise is similar to 2002 VE95. In summary, we find that Pholus is the only object in our survey for which the inclusion of a third component, CH_3OH, significantly improved the fit.

We detected water ice, that is f greater than 0, on 4 out of the 12 Centaurs and 12 of the 33 KBOs at the 3σ level or higher. An additional 2 Centaurs and 4 KBOs have 1σ detections of water ice on their surfaces. In our modeling, we find that the family members of 2003 EL61 are distinguished from the general KBO population by significantly higher fractions of water ice in their spectra, f and the negative (blue) values for the slope of the NIR continuum, m. The four members of the 2003 EL61 collisional family in our survey, 1995 SM55, 2002 TX300, 2003 OP32, and 2005 RR43, as well as 2003 EL61 itself have a mean f of 0.93 and a standard deviation of 0.07. In contrast, the rest of the sample has values of f less than 0.55. Given that the family members are likely not representative of the general KBO population, we will treat these objects separately below and then return to the discussion of the spectral properties of the general population.

To best characterize the spectra, we allow the fraction of water ice in the spectrum to take on negative values in our modeling, effectively creating the inverse of the water ice spectral features. The aim was to discover if additional spectral characteristics could be identified. We find that five objects, Chaos, 1999 RZ253, 2002 KX14, 2005 RN43, and K50830B, have negative f values to within 1σ, but not within the 3σ errors. These objects appear to have broad dips in their reflectance between 1.7 and 2.0 μm. This region straddles the telluric 1.8 μm water line and the dip may be due to poor correction of the telluric line as at least three of the objects, 2002 KX14, 2005 RN43, and K50830B, were observed under variable weather conditions and their spectra are likely to have systematic errors.

Table 2
Spectral Parameters

	Name	Tax. G[a]	Vis Gradient[b]	NIR Gradient (m)[c]	f[d]	Depth[e]	χ^2_υ[f]	Ices Prev. Detected[g]	References
				Kuiper Belt Objects					
1	15875 (1996 TP66)	RR	30.61 ± 4.45	$-3.76^{+0.45}_{-0.47}$	$-0.11^{+0.16}_{-0.18}$	$-0.03^{+0.04}_{-0.04}$	1.22	...	1
2	19521 Chaos (1998 WH24)	IR	23.44 ± 3.34	$-1.86^{+0.09}_{-0.26}$	$-0.44^{+0.06}_{-0.06}$	$-0.12^{+0.04}_{-0.02}$	1.85	...	2
3	20000 Varuna (2000 WR106)	IR	27.18 ± 2.95	$-1.86^{+0.17}_{-0.17}$	$-0.04^{+0.06}_{-0.06}$	$-0.01^{+0.02}_{-0.02}$	1.07	H_2O	2,3
4	24835 (1995 SM55)[h]	BB	2.41 ± 2.88	$4.89^{+1.50}_{-1.50}$	$0.90^{+0.04}_{-0.04}$	$0.56^{+0.06}_{-0.06}$	1.11	...	1
5	26181 (1996 GQ21)	RR	37.37 ± 2.85	$-1.50^{+0.18}_{-0.18}$	$0.24^{+0.06}_{-0.06}$	$0.09^{+0.02}_{-0.02}$	1.32	None	1,4
6	26375 (1999 DE9)	IR	20.64 ± 2.35	$-3.33^{+0.30}_{-0.30}$	$-0.07^{+0.08}_{-0.10}$	$-0.02^{+0.02}_{-0.02}$	1.41	H_2O	1, 5
7	28978 Ixion (2001 KX76)	IR/RR	23.44 ± 2.06	$-1.01^{+0.23}_{-0.24}$	$0.17^{+0.08}_{-0.08}$	$0.06^{+0.04}_{-0.04}$	1.09	Possible H_2O	1, 6, 7
8	33340 (1998 VG44)	IR	20.67 ± 3.49	$-3.85^{+0.78}_{-0.78}$	$-0.17^{+0.32}_{-0.38}$	$-0.05^{+0.10}_{-0.10}$	1.08	...	2
9	38628 Huya (2000 EB173)	IR	24.09 ± 4.73	$-1.64^{+0.09}_{-0.09}$	$-0.04^{+0.04}_{-0.04}$	$-0.01^{+0.02}_{-0.02}$	2.21	Possible H_2O	1,5, 8, 9
10	42301 (2001 UR163)	RR	53.03 ± 6.70	$0.15^{+0.65}_{-0.65}$	$-0.01^{+0.22}_{-0.32}$	$-0.00^{+0.08}_{-0.10}$	1.17	...	10
11	47171 (1999 TC36)	RR	31.80 ± 2.22	$-1.16^{+0.16}_{-0.16}$	$0.21^{+0.06}_{-0.06}$	$0.08^{+0.02}_{-0.02}$	1.27	H_2O	10, 11, 12
12	47932 (2000 GN171)	IR	25.55 ± 2.61	$0.30^{+0.22}_{-0.22}$	$-0.10^{+0.14}_{-0.16}$	$-0.03^{+0.04}_{-0.04}$	0.95	None	1, 9
13	50000 Quaoar (2002 LM60)	RR?	27.55 ± 0.20	$0.47^{+0.03}_{-0.04}$	$0.49^{+0.02}_{-0.02}$	$0.21^{+0.00}_{-0.00}$	2.56	H_2O	13, 14
14	55565 (2002 AW197)	IR	22.48 ± 7.32	$0.75^{+0.16}_{-0.16}$	$0.08^{+0.06}_{-0.08}$	$0.03^{+0.02}_{-0.02}$	1.52	H_2O	2, 15
15	55636 (2002 TX300)[h]	BB	0.00 ± 1.30	$-27.33^{+1.94}_{-1.94}$	$0.97^{+0.01}_{-0.01}$	$0.64^{+0.01}_{-0.00}$	1.13	H_2O	16, 17
16	55637 (2002 UX25)	IR	20.64 ± 2.26	$-0.20^{+0.14}_{-0.14}$	$0.06^{+0.08}_{-0.08}$	$0.02^{+0.02}_{-0.02}$	1.31	...	10
17	55638 (2002 VE95)	RR	38.81 ± 2.59	$0.98^{+0.07}_{-0.07}$	$0.23^{+0.02}_{-0.02}$	$0.09^{+0.02}_{-0.02}$	1.78	H_2O, CH_3OH	2?, 18
18	66652 (1999 RZ253)	RR	28.67 ± 3.61	$-5.24^{+0.72}_{-0.72}$	$-0.72^{+0.60}_{-0.64}$	$-0.17^{+0.14}_{-0.12}$	1.14	...	2?
19	84522 (2002 TC302)	...	33.72 ± 2.50	$1.65^{+0.37}_{-0.37}$	$0.23^{+0.10}_{-0.12}$	$0.09^{+0.04}_{-0.04}$	1.21	...	1
20	84922 (2003 VS2)	...	24.08 ± 2.32	$-0.50^{+0.10}_{-0.15}$	$0.18^{+0.04}_{-0.04}$	$0.07^{+0.02}_{-0.02}$	1.41	...	10
21	119951 (2002 KX14)	...	26.42 ± 2.37	$-0.28^{+0.26}_{-0.26}$	$-0.67^{+0.58}_{-0.66}$	$-0.17^{+0.12}_{-0.10}$	1.12	...	10
22	120132 (2003 FY128)	...	...	$-2.61^{+0.96}_{-1.17}$	$0.18^{+0.72}_{-0.21}$	$0.07^{+0.16}_{-0.16}$	1.29	...	...
23	120178 (2003 OP32)[h]	BB?	−1.09 ± 2.20	$42.42^{+2.19}_{-0.74}$	$1.04^{+0.01}_{0.01}$	$0.74^{+0.00}_{0.00}$	...	19	
24	120348 (2004 TY364)	...	...	$0.99^{+0.16}_{-0.15}$	$0.10^{+0.06}_{-0.06}$	$0.04^{+0.02}_{-0.02}$	1.14	...	...
25	136108 (2003 EL61)[h]	BB	−0.17 ± 1.78	$-10.68^{+0.19}_{-0.22}$	$0.83^{+0.01}_{-0.01}$	$0.48^{+0.00}_{-0.00}$	2.05	H_2O	20, 21,22
26	136472 (2005 FY9)	BR	...	$-6.39^{+0.13}_{0.00}$	...	...	...	CH_4, C_2H_6	23, 24
27	145452 (2005 RN43)	...	...	$-0.24^{+0.13}_{-0.14}$	$-0.11^{+0.08}_{-0.10}$	$-0.03^{+0.02}_{-0.02}$	1.05	...	...
28	145453 (2005 RR43)[h]	...	...	$-28.64^{+1.07}_{-2.52}$	$0.97^{+0.01}_{-0.01}$	$0.65^{+0.02}_{-0.00}$	1.84	H_2O	25
29	2003 AZ84	BB	2.23 ± 0.87	$-1.53^{+0.28}_{-0.48}$	$0.42^{+0.06}_{-0.06}$	$0.18^{+0.04}_{-0.04}$	1.20	...	13
30	2004 NT33	...	...	$1.26^{+0.38}_{-0.38}$	$0.10^{+0.05}_{-0.07}$	$0.03^{+0.01}_{-0.01}$	2.72	...	...
31	2004 PG115	...	...	$0.62^{+0.28}_{-0.28}$	$0.25^{+0.07}_{-0.07}$	$0.10^{+0.02}_{-0.01}$	1.27	...	...
32	2005 QU182	...	...	$1.43^{+0.26}_{-0.26}$	$-0.31^{+0.14}_{-0.16}$	$-0.09^{+0.02}_{-0.02}$	1.63	...	...
33	2005 UQ513	...	...	$0.12^{+0.20}_{-0.20}$	$0.18^{+0.07}_{-0.07}$	$0.06^{+0.01}_{-0.01}$	1.26	...	...
				Centaurs					
34	2060 Chiron (1977 UB)	BB	−0.07 ± 1.35	$1.35^{+0.12}_{-0.12}$	$0.02^{+0.02}_{-0.02}$	$0.01^{+0.00}_{-0.00}$	3.52	H_2O	1, 26,27,28
35	5145 Pholus (1992 AD)	RR	48.42 ± 2.37	$-2.20^{+0.08}_{-0.08}$	$0.24^{+0.02}_{-0.02}$	$-0.02^{+0.00}_{-0.00}$	4.94	H_2O, CH_3OH	1, 29
36	8405 Asbolus (1995 GO)	BR	13.60 ± 2.96	$-0.30^{+0.22}_{-0.22}$	$-0.03^{+0.03}_{-0.05}$	$-0.01^{+0.01}_{-0.01}$	1.67	None	1, 30, 31, 32
37	10199 Chariklo (1997 CU26)	BR	13.03 ± 1.10	$0.19^{+0.05}_{-0.05}$	$0.33^{+0.01}_{-0.01}$	$0.13^{+0.00}_{-0.00}$	3.91	H_2O	1, 33,34
38	29981 (1999 TD10)	BR	13.25 ± 2.27	$-0.59^{+0.09}_{-0.09}$	$-0.04^{+0.02}_{-0.02}$	$-0.01^{+0.00}_{-0.00}$	1.76	...	1
39	31824 Elatus (1999 UG5)	RR	26.01 ± 2.74	$1.16^{+0.37}_{-0.37}$	$0.04^{+0.04}_{-0.04}$	$0.01^{+0.01}_{-0.01}$	1.14	H_2O	1, 35
40	52872 Okyrhoe (1998 SG35)	BR	11.23 ± 3.84	$0.17^{+0.20}_{-0.20}$	$0.11^{+0.08}_{-0.09}$	$0.04^{+0.02}_{-0.02}$	1.32	H_2O ?	1, 11
41	54598 Bienor (2000 QC243)	BR	8.50 ± 3.21	$-0.20^{+0.60}_{-0.60}$	$0.11^{+0.11}_{-0.11}$	$0.04^{+0.02}_{-0.02}$	1.08	H_2O	1,11
42	65489 Ceto (2003 FX128)	...	20.64 ± 3.39	$-1.65^{+0.27}_{-0.33}$	$0.34^{+0.08}_{-0.08}$	$0.14^{+0.04}_{-0.04}$	1.14	...	1
43	83982 Crantor (2002 GO9)	RR	39.55 ± 2.89	$-1.29^{+0.41}_{-0.41}$	$0.29^{+0.06}_{-0.05}$	$0.11^{+0.01}_{-0.01}$	1.22	H_2O	1, 15

Table 2
(Continued)

	Name	Tax. G[a]	Vis Gradient[b]	NIR Gradient (m)[c]	f[d]	Depth[e]	χ_υ^{2}[f]	Ices Prev. Detected[g]	References
44	95626 (2002 GZ32)	...	28.23 ± 4.24	$-4.08^{+4.14}_{-3.83}$	$-0.37^{+0.77}_{-2.15}$	$-0.10^{+0.02}_{-0.01}$	0.95	...	...
45	127546 (2002 XU93)	...	...	$-0.30^{+1.54}_{-1.54}$	$0.08^{+0.32}_{-0.50}$	$0.03^{+0.06}_{-0.08}$	1.36	...	...

Notes.
[a] The Taxonomic groups as defined in Barucci et al., 2005; BB: blue, BR: intermediate blue red, IR: moderately red, RR: red.
[b] The visible (500–800 nm) color gradient in % change in reflectance per 100 nm, calculated using the methods in Hainaut & Delsanti (2002).
[c] The NIR (1.5–2.4 μm) color gradient in % change in reflectance per 100 nm found from slope of the continuum component (m) used to fit the spectral model.
[d] The fraction of water ice in the spectrum.
[e] The fractional depth of the 2.0 μm to 1.7 μm spectral regions, where larger depth indicates stronger water ice spectral signatures. The depth is shown here for comparison with previous studies (e.g. Brown et al (2007a, 2007b)). The depth is calculated using the fitted model spectrum rather than the data to reduce the noise and has had the continuum contribution subtracted out.
[f] The reduced χ^2 value of the spectral model fit to the data.
[g] Spectral features identified in the NIR spectra by other authors.
[h] 2003 EL61 and its associated family members.
References. (1) Hainaut & Delsanti (2002); (2) Barucci et al. (2005); (3) Licandro, et al. (2001); (4) Doressoundiram et al. (2003); (5) Jewitt & Luu (2001); (6) Licandro et al. (2002); (7) Boehnhardt et al. (2004); (8) Brown et al. (2000); (9) de Bergh et al. (2004); (10) Tegler, et al. (in preparation) Available at http://www.physics.nau.edu/~tegler/research/survey.htm; (11) Dotto et al. (2003); (12) Merlin et al. (2005); (13) Fornasier et al. (2004); (14) Jewitt & Luu (2004); (15) Doressoundiram et al. (2005); (16) Doressoundiram et al. (2005); (17) Licandro et al. (2006); (18) Barucci et al. (2006); (19) Rabinowitz, Schaefer & Tourtellotte (2007); (20) Rabinowitz et al. (2006); (21) Trujillo et al. (2007); (22) Merlin et al. (2007); (23) Licandro et al. (2006); (24) Brown et al. (2007); (25) Pinilla-Alonso et al. (2007); (26) Luu et al. (2000); (27) Foster et al. (1999); (28) Romon-Martin et al. (2003); (29) Cruikshank et al. (1998); (30) Barucci et al. (2000); (31) Brown (2000); (32) Romon-Martin et al. (2002); (33) Brown & Koresko (1998); (34) Dotto et al. (2003); (35) Bauer et al. (2002).
(Spectral data for all objects in our survey are available as a supplemental data file in the online journal and at http://www.gps.caltech.edu/~pa/data.html.)

Phyllosilicates and other silicate materials have spectral features at 1.9 μm, but these minerals do not reproduce the broad dip that extends to the region of 1.7 μm in the spectrum. We also note that our model produces negative f values for spectra dominated by methane bands like that of 2005 FY9, though there is no indication that methane exists on the five objects listed above.

5.1. The 2003 EL61 Collisional Family

All the objects in our survey with the strongest signatures of water ice, that is f greater than 0.55, have previously been shown to be dynamically related to 2003 EL61 and are likely 100–300 km sized fragments ejected from its mantle during a massive collision. The evidence for the giant impact and the formation of the fragments as well as their general spectral characteristics are discussed in Brown et al. (2007b). Ragozzine & Brown (2007) discuss the dynamical nature of this family and find that the collision is over one billion years old and likely primordial. Here we discuss in greater detail their spectroscopic features.

In addition to the deep water ice absorption features, the family members have uniformly neutral color in the visible. This contrasts with the general KBO population, which shows a diversity of color but is generally red (Figure 8), typically attributed to the presence of irradiated organics (Strazzulla et al. 1991; Hansen & McCord 2004). The neutral visible colors are consistent with a relatively pure water ice surface but may also indicate a low abundance of the simple ices and organic materials from which tholins are formed. The model fits of the family members revealed that a second, blue continuum component significantly decreased the minimum χ^2 value with the exception of 2003 OP32. The blue component could be an artifact of modeling with a fixed grain size that is too small. Larger grain sizes would produce a slightly bluer water ice spectrum. To determine if the blue component is required by the data, we created more complex models involving both intimate and geographically mixed water ices of varying grain sizes but were unable to reproduce the observed spectra. As such, the blue continuum component appears to be a real feature in the spectra of most of the family members. The slope of the component is varied, which may reflect the normalization rather than intrinsic

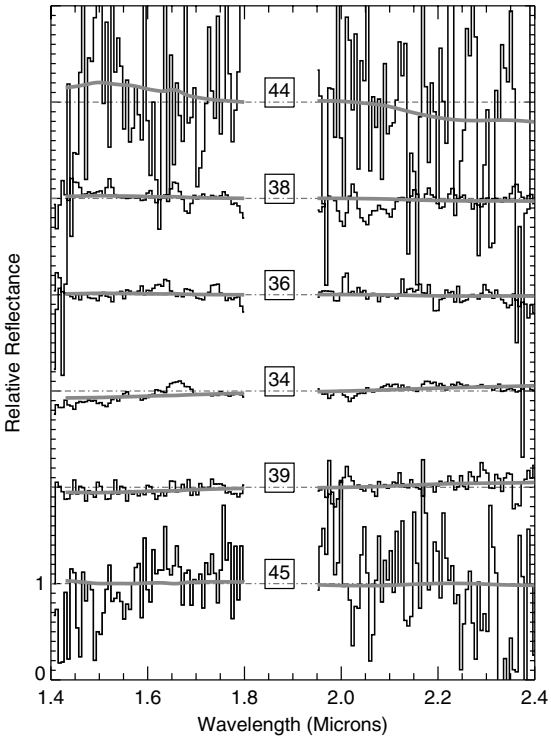

Figure 7. The relative reflectance spectra for the following Centaurs—45: 2002 XU93, 39: Elatus, 34: Chiron, 36: Asbolus, 38: 1999TD10, 44: 2002GZ32. The spectra are shown in decreasing fraction of water ice from bottom to top. No water ice was detected in our data for these Centaurs.

Table 3.
Physical Parameters

	Name	H	p_v (%)[a]	D (km)	a (AU)	Ecc	Inc (deg)	q (AU)	References
				Kuiper Belt Objects					
1	15875 (1996 TP66)	6.8	7.4^{+7}_{-3}	160^{-45}_{+45}	39.21	0.33	5.7	26.35	1
2	19521 Chaos (1998 WH24)	4.9	>5.8	<747	45.59	0.10	12.1	40.94	2, 3
3	20000 Varuna (2000 WR106)	3.7	16^{+10}_{-8}	500^{-100}_{+100}	42.95	0.05	17.2	40.72	1
4	24835 (1995 SM55)[a]	4.8	>6.7	<704	41.65	0.10	27.1	37.36	2, 3
5	26181 (1996 GQ21)	5.2	...	...	95.06	0.597	13.3	38.31	...
6	26375 (1999 DE9)	4.7	$6.85^{+1.58}_{-1.19}$	$461.0^{-45.3}_{+46.1}$	55.85	0.42	7.60	32.34	1
7	28978 Ixion (2001 KX76)	3.2	12^{+14}_{-6}	650^{-220}_{+260}	39.62	0.24	19.6	30.072	1
8	33340 (1998 VG44)	6.5	...	...	39.14	0.25	3.0	29.35	...
9	38628 Huya (2000 EB173)	4.7	$5.04^{+0.5}_{-0.41}$	$532.6^{-24.4}_{+25.1}$	39.75	0.28	15.5	28.54	1
10	42301 (2001 UR163)	4.2	...	...	51.35	0.284	0.80	36.7666	...
11	47171 (1999 TC36)	4.9	$7.18^{+1.53}_{-1.17}$	$414.6^{-38.2}_{+38.8}$	39.23	0.22	8.4	30.56	1
12	47932 (2000 GN171)	6.0	$5.68^{+2.54}_{-1.59}$	$321.05^{-54.2}_{+57.4}$	39.72	0.29	10.8	28.28	1
13	50000 Quaoar (2002 LM60)	2.6	9 ± 3	1260 ± 190	43.54	0.03	8.0	42.02	1, 4
14	55565 (2002 AW197)	3.3	$11.77^{+4.42}_{-3.00}$	$734.6^{-108.3}_{+116.4}$	47.37	0.13	24.4	41.16	1
15	55636 (2002 TX300)[a]	3.3	>19	<709	43.08	0.123	25.9	37.78	3, 5
1	55637 (2002 UX25)	3.6	$11.50^{+5.09}_{-3.09}$	$681.2^{-114.0}_{+115.6}$	42.52	0.142	19.5	36.48	1
17	55638 (2002 VE95)	5.3	...	...	39.15	0.285	16.4	27.9923	...
18	66652 (1999 RZ253)	5.9	29 ± 12	170 ± 39	43.72	0.09	0.60	39.83	2, 3
19	84522 (2002 TC302)	3.9	$3.1^{+2:9}_{-1:2}$	1150^{325}_{+337}	55.03	0.29	35.1	39.02	1
20	84922 (2003VS2)	4.2	...	...	39.28	0.073	14.8	36.41	...
21	119951 (2002 KX14)	4.4	...	...	39.00	0.041	0.40	37.40	...
22	120132 (2003 FY128)	5.0	...	...	49.700	0.25	11.8	37.09	...
23	120178 (2003 OP32)[a]	4.1	...	...	43.18	0.107	27.2	38.56	...
24	120348 (2004TY364)	4.5	...	...	38.7	0.067	24.9	36.11	...
25	136108 (2003 EL61)[a]	0.20	$84.^{+10}_{-20}$	1150^{-150}_{+150}	43.33	0.19	28.2	35.14	1, 6
26	136472 (2005FY9)	−0.30	$80.^{+10}_{-20}$	1500^{-200}_{+300}	45.71	0.15	29.0	38.62	1
27	145452 (2005 RN43)	3.9	...	...	41.53	0.02	19.29	40.62	...
28	145453 (2005 RR43)[a]	4.0	...	...	43.05	0.14	28.54	37.19	...
29	2003 AZ84	3.9	$12.32^{+4.31}_{-2.91}$	$685.8^{-95.5}_{+98.8}$	39.50	0.179	13.6	32.43	1
30	2004 NT33	...	...	...	43.44	0.15	31.22	36.85	...
31	2004 PG115	...	...	...	89.83	0.59	16.28	36.42	...
32	2005 QU182	...	...	...	126.4	0.72	14.00	35.39	...
33	2005 UQ513	...	...	...	43.336	0.14	25.72	36.84	...
				Centaurs					
34	2060 Chiron (1977 UB)	6.5	$7.57^{+1.03}_{-0.87}$	$233.3^{-14.4}_{+14.7}$	13.701	0.38	6.9	8.45	1
35	5145 Pholus (1992 AD)	7.0	8.0^{+7}_{-3}	140^{-40}_{+40}	20.411	0.57	24.7	8.74	1
36	8405 Asbolus (1995 GO)	9.0	$5.46^{+1.27}_{-0.86}$	$84.2^{-7.8}_{+7.8}$	18.02	0.621	17.6	6.82	1
37	10199 Chariklo (1997 CU26)	6.4	$5.73^{+0.49}_{-0.42}$	$258.6^{-10.3}_{+10.3}$	15.854	0.175	23.4	13.07	1
38	29981 (1999 TD10)	8.8	$4.40^{+1.42}_{-0.96}$	$103.7^{-13.5}_{+13.6}$	94.97	0.87	6.0	12.25	1
39	31824 Elatus (1999 UG5)	10.1	10^{+4}_{-3}	$30+^{-8}_{+8\|}$	11.769	0.38	5.3	7.27	1
40	52872 Okyrhoe (1998 SG35)	11.3	$2.49^{+0.81}_{-0.55}$	$52.1^{-6.9}_{+6.9}$	8.38	0.308	15.6	5.79	1
41	54598 Bienor (2000 QC243)	7.6	$3.44^{+1.27}_{-0.82}$	$206.7^{-30.1}_{+30.1}$	16.48	0.200	20.7	13.15	1
42	65489 Ceto (2003 FX128)	6.3	$7.67^{+1.38}_{-1.10}$	$229.7^{-18.2}_{+18.6}$	103.00	0.83	22.3	17.82	1
43	83982 Crantor (2002 GO9)	9.1	11^{+7}_{-4}	60^{-13}_{+15}	19.537	0.28	12.8	10.92	1
44	95626 (2002 GZ32)	6.8	...	...	23.196	0.223	15.0	18.06	1
45	127546 (2002 XU93)	7.9	...	...	66.950	0.687	78.0	20.95	1

Note.
[a] 2003 EL61 and its associated family members.

References. (1) Stansberry et al. (2007); (2) Altenhoff et al. (2004); (3) Grundy et al. (2005); (4) Brown & Trujillo (2004); (5) Ortiz et al. (2004); (6) Rabinowitz et al. (2006).

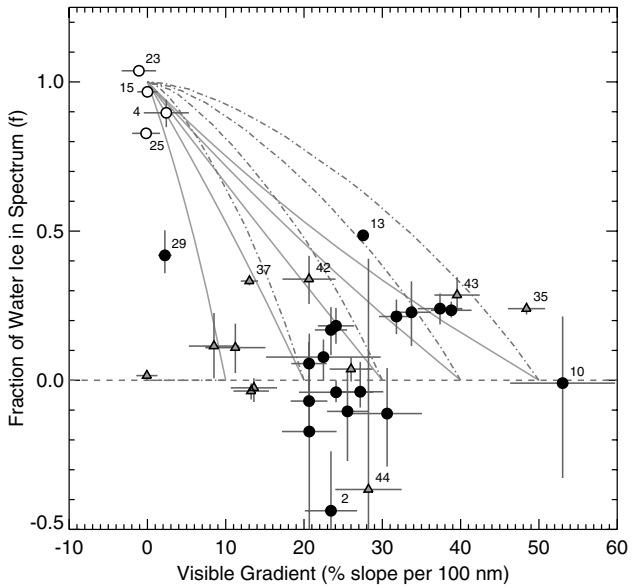

Figure 8. The fraction of water ice detected in the spectrum versus the visible color gradient for KBOs (black circles) and Centaurs (gray triangles). 2003 EL61 and its collisional family are represented by white circles. The errors are the 3σ error bars. Objects of interest are labeled with numbers as they appear in tables. The thick gray lines represent the expected distribution for a two-component system where water ice and a featureless continuum are the end members and are mixed geographically (see Section 5.2). The different lines represent different color gradients for the featureless component. The dashed gray lines represent intimate mixtures of the two components. Once the collisional family of 2003 EL61 is excluded, no correlation is found between the fraction of water ice detected in the spectrum of KBOs and Centaurs and their visible colors.

differences between the objects. In an attempt to identify the blue component, we examined the spectra for additional features, but we find no evidence for additional absorptions in the spectra. A similar blue component was reported by Trujillo et al. (2007) for 2003 EL61 and by Pinilla-Alonso et al. (2007) for 2005 RR43. In the case of 2003 EL61, HCN and phyllosilicate clays were both proposed as possible sources of the blue continuum component, but no positive identification was possible.

While it is difficult to determine much physical information for the blue continuum component without better data, the spectra do provide a few clues about the physical state of water ice on the surface. The 1.65 μm crystalline water ice feature is evident in all the spectra of family members. The crystal structure of water ice is expected to be destroyed by high energy particles and solar radiation on time scales short compared to the age of the family (Strazzulla et al. 1991; Hansen & McCord 2004; Kouchi & Kuroda 1990), causing the 1.65 μm feature to disappear. However, crystalline water ice is reported on surfaces of icy satellites as well as icy KBOs when spectra of sufficient signal to noise are available, suggesting that a general process is likely acting to maintain the crystallinity of the water ice surfaces. Both thermal and nonthermal mechanisms have been proposed as a means to reform crystalline ice on these bodies. Cryovolcanism and outgassing, where surface materials are heated well above the crystallization temperatures of $\sim$100 K, have been proposed for bodies like Quaoar (Jewitt & Luu 2004). Grundy et al. (2006) and Brown & Calvin (2000) have proposed maintaining crystalline ice through nonthermal processes such as slow vapor deposition from micrometeorite bombardment and nonthermal energy input from radiation. The presence of crystalline water ice on the family members appears to preclude thermal processes as the primary crystallization mechanism. KBOs with diameters less than 300 km are not expected to have sufficient geothermal energy to produce crystalline water ice near or at their surfaces. As such, we argue that the processes of crystallizing water ice on these objects is nonthermal in nature. In the future, we expect that any water ice detected on the surface of a KBO will be in the crystalline form regardless of size of the KBO.

In addition to the crystalline feature, the large depths of the 1.5 and 2.0 μm overtone features suggest that the grain size is larger for some of the members of the family than is often measured on KBOs. Though the grain size may not represent the true crystal grain size of the ice, it can be used to judge the relative grain structures and impurities between objects. Using the models for a water ice surface that include scattering developed for Orcus and 2003 EL61 (Trujillo et al. 2005; 2007), we find that the grain sizes are between 100–125 μm on 2002 1995 SM55, 2002 TX300 and 2005 RR43—larger than is typically found for KBOs (Barucci et al. 2007). The water ice on 2003 OP32 was found to have a grain size of 60 μm, similar to the grain size that Trujillo et al. (2007) found for 2003 EL61. The larger grain sizes on the family members may be consistent with water ice surfaces where the crystals have grown due to fewer impurities (Brown et al. 2007a).

From the spectra alone, it is difficult to infer specific details about the giant impact on proto-2003 EL61 as many of the parameters are poorly constrained or ambiguous. The large fraction of water ice detected on the family members could indicate that the proto 2003 EL61 was differentiated with material ejected largely from an icy mantle. Additionally, the spectral evidence is consistent with heating of the fragments during the impact, leading to devolatilization of carbon-bearing species, but the spectral signatures could be explained by other processes. With this in mind, the spectral characteristics may be best interpreted as identifying markers for the family members.

5.2. KBOs and Centaurs

A two-component surface, with water ice as one end member and a dark, red, carbon-rich material at the other, could explain the variety of visible colors and variable presence of water ice seen on KBOs (e.g., Barucci et al. 2005). In such a model, the measured f should correlate with the visible colors. In Figure 8, we see that there is little correlation between these parameters for either the KBO or the Centaur population. The colors of KBOs and Centaurs show no clear trend with f and are often variable amongst objects with similar f values. For example, 2003 AZ84 and Quaoar show similar degrees of water ice on their surfaces but 2003 AZ84 is neutral while Quaoar is moderately red. Barucci et al. (2005) argue that KBOs and Centaurs can be organized into four separate color groups (BB, BR, IR, and RR). We find that all the 2003 EL61 collisional family members fall into the bluest group (BB) as well as 2003 AZ84, suggesting that this group strongly correlates with the presence of water ice on the surface (Figure 9). The remaining objects in our survey are distributed among the three other taxonomic groups: BR, IR, and RR. We find no correlation between the remaining three taxonomic groups and any NIR spectral characteristics we measured for our spectra. Specifically, we find that the fraction of water ice in the spectrum can vary widely amongst the objects in a particular group and that the groups have similar distributions of f with the exception of the BB group. As such, we do not anticipate that

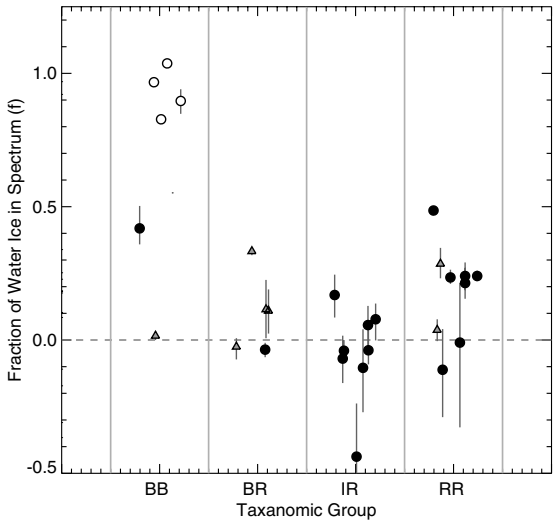

Figure 9. The fraction of water ice detected in the spectrum versus the taxonomic group for KBOs (black circles) and Centaurs (gray triangles). 2003 EL61 and its family are presented by white circles. The taxanomic designations are based on an analysis of the visible and NIR photometric colors and are directly from Barucci et al. (2005). Each object has been offset to make them more easily distinguishable. We find that the BB (blue) group is generally well correlated with the presence of significant detections of water ice in the spectrum since this group is dominated by the 2003 EL61 collisional family members. Of the remaining groups, RB (red–blue), IR (intermediate red), and RR (red), we find no correlation with the fraction of water ice detected in the spectrum. As such these taxonomic groups do not appear to correspond to specific spectral signatures in our NIR spectra.

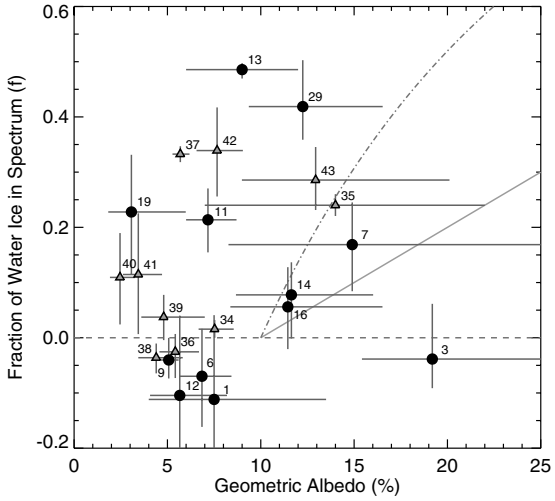

Figure 10. The fraction of water ice detected in the spectrum versus the albedo for KBOs (black circles) and Centaurs (gray triangles). 2003 EL61 is not shown, but has an albedo of 84^{+10}_{-20} and an f of $0.83^{+0.01}_{-0.01}$. The albedos are from Stansberry et al. (2007). Objects of interest are labeled with numbers as they appear in tables. We find no correlation in the fraction of water ice detected in the spectrum and the albedo measured for the object. The thick gray line represents the expected albedo for a given surface fraction of water ice and is determined from our two-component synthetic surface model. In the model we assume water ice with at 60% albedo and a dark, featureless material with a *V*-band albedo of 10% mix geographically in various ratios. The dashed line represents the distribution expected for an intimate mixture of the two components.

these taxonomic groups will yield specific information about the surface characteristics above predicting the likelihood of the presence of ices for objects in the BB group.

Though we do not physically model the surfaces of the KBOs and Centaurs in our survey, we can use models of simulated surfaces to predict trends that could be detected in the parameterization of a population of spectra. We created artificial spectra of idealized, two-component surfaces with varying ratios of water ice and a featureless component that represents carbon-rich material. We assume properties of the water ice and the featureless component based on those observed on icy bodies. The water ice reflectance was modeled in the NIR using the optical constants from Grundy & Schmitt (1998) and assuming isotropic scattering. We assumed a 60% albedo for the visible portion of the water ice reflectance and a grain size of 50 μm was used. The carbon-rich component is far less characterized, however, so we created a family of models assuming different properties for the carbon-rich end member. We assumed that the visible gradient varied between 10% per 100 nm and 50% per 100 nm, which are typical values of the gradients measured on KBOs (Hainaut & Delsanti 2002). The average NIR gradient, m, that we measured in our own data was much smaller than the visible gradient and therefore we set m to 0 for our synthetic carbon-rich component. The carbon-rich component was given an albedo of 10% at 550 nm, which is the average albedo of the ice-free objects in our survey (Stansberry et al. 2007). Since the surfaces of KBOs could be mixed either intimately or geographically, we consider both cases. In these simulations, we tacitly assume that while the carbon-rich component may be a mixture of materials, it is the same for all objects and that this material does not alter over time. For intimate mixtures we use our assumed reflectance for the carbon-rich component to calculate its single scattering albedos. The intimate mixture models were created by linearly mixing the single scatter albedos of water ice and the carbon-rich material and calculating the resulting reflectance using the equations of radiative transfer from Hapke (1993). The synthetic NIR spectrum is then analyzed to determine f and m using the same methods used for the real spectra and the visible color gradient is calculated using the methods described in Hainaut & Delsanti (2002). Figure 8 shows the measured G_v and f for the synthetic surfaces.

We see that our results for the KBOs and Centaurs do not follow any of the models produced above, indicating that the surfaces of these objects are not well described by our synthetic two-component surface model. While the exact f and m measured for our synthetic data depend on poorly known parameters such as the albedo, the overall trends that our simple surface modeling predicts should be similar regardless of the parameters of the modeling. Even a model in which the carbon-rich material reddens or the grain size is altered over time cannot explain the data if this material increasingly obscures the water ice.

The relationship between the albedo of the objects and f further suggests that a simple mixing of two components does not describe the surface of KBOs or Centaurs well. The albedos of KBOs are diverse, ranging from ~4% up to ~80% (Stansberry et al. 2007, in press). The dwarf planet-sized KBOs have the highest albedos likely due to resurfacing of CH_4 or N_2 through atmospheric deposition (Stansberry et al. 2007; Brown et al. 2005). In our sample, 17 KBOs and 10 Centaurs have measured albedos. If we exclude the methane giants and the KBOs in the collisional family of 2003 EL61, we find that there is no significant correlation between f and albedo of either KBOs or Centaurs using a Kendall rank-correlation test (see Figure 10). In some cases, we see that objects like 1999 TC36

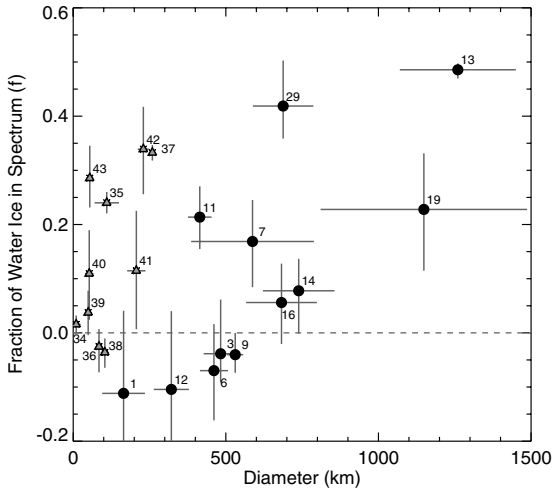

Figure 11. The fraction of water ice detected in the spectrum versus the diameter of KBOs (black circles) and Centaurs (gray triangles). The objects are labeled with numbers corresponding to their appearance in the tables. We find a correlation between the size and the degree of water ice detected for KBOs. A Kendall rank correlation gives a correlation coefficient of 0.5 with a probability of obtaining this value for a random data set of 1%. A similar correlation is not seen for Centaurs.

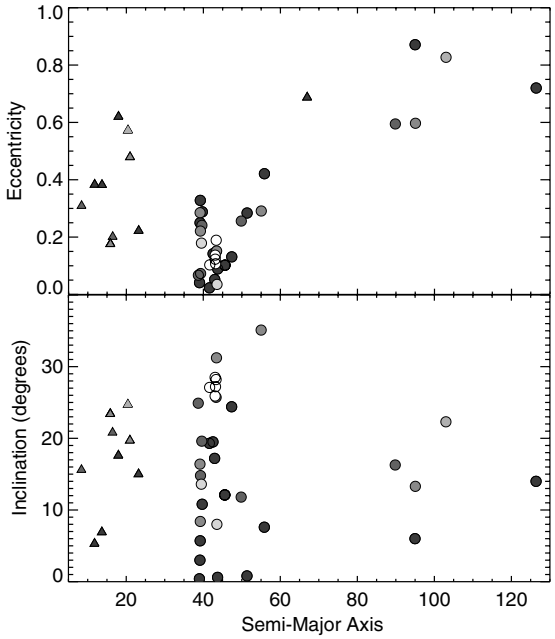

Figure 12. The orbital parameters of objects in our survey. KBOs are represented by circles and Centaurs by triangles. Shading represents the fraction of water ice in the spectrum, f. The white data points are objects with $f > 0.4$, medium gray have $0.4 < f > 0.2$, and dark gray have $f < 0.2$. The white objects are concentrated in orbits near 2003 EL61 and are the collisional family members. The remaining objects with moderate water ice detection are scattered throughout the trans-Neptunian region. Once the 2003 EL61 family is discarded, we find no correlation between the NIR spectral properties of the objects in our survey and their orbital parameters.

have significant detections of water ice on their surfaces but have low albedos, 7%. Again, using the same two-component synthetic surface models described above, we calculated the expected visual albedo as a function of f (Figure 10). It is apparent that our two-component description of the surface fails to describe the data and that any new formulation of the surface characteristics must allow for a variety of albedos for a given abundance of water ice.

While there appear to be no clear trends in the colors or the albedos of KBOs and Centaurs and fraction of water ice in their spectra, we do find that there may be a correlation in the KBO population between f and the diameter. A Kendall rank-correlation test gives a correlation coefficient of 0.5 with a probability of obtaining this correlation coefficient for a random data set of 1%. Barucci et al. (2007) noted this trend for the largest KBOs, but Figure 11 shows that this trend nominally extends down to moderate-sized KBOs in our survey and is not the result of observational bias against detecting water ice on smaller objects with lower signal-to-noise spectra. This trend may indicate that the formation of water ice on the surface is geophysically controlled as larger objects have greater heat from accretional energy and radiogenic materials than smaller objects. The higher heat available would make it more likely for these objects to experience geothermal processes, though there is no indication of recent geological activity.

However, we do not detect a correlation between size and the fraction of water ice in our sample of Centaurs. In contrast to the KBO population, we find that Centaurs of similar sizes can have a wide range in water ice abundances on their surfaces. This suggests that the processes that control the presence of water ice on the surface of Centaurs could be different than those on KBOs. We investigated if a mechanism relating to the far warmer temperatures on Centaurs may be responsible by examining the relation of f with perihelion distance. There too, a Kendall rank correlation test gives no significant correlation between the perihelion distance and f.

In general, we find no correlation between the NIR surface characteristics and the orbital elements of the KBOs or Centaurs in our population other than what has been previously noted for the collisional family of 2003 EL61 (Brown et al. 2007b). Figure 12 shows that the orbital elements of our sample with both icy and non-icy objects are evenly distributed through the Kuiper belt's hot classical and scattered populations. As such, we conclude that no correlation seems to exist amongst the KBO orbital parameters for these dynamical populations and f above what has been previously been noted for the 2003 EL61 family.

Finally, the coincidence between icy surfaces and moon-forming collisions on 2003 EL61 and Pluto prompted us to examine if this trend extends to the other icy KBOs. We note that a number of objects in our survey with significant water ice absorptions including 2003 AZ84, Quaoar, 2003 TC36, and Ceto have satellites or are binary (Noll et al. 2007). Orcus, while not in our survey, also fits with this trend. It may be that collisions emplaced water ice on the surfaces of these objects, but the spectra offer no definitive indications of a particular mechanism. Alternatively, 2002 UX25 has a satellite but shows no signatures of water ice. With these limited data, it is unclear what trend, if any, exists between collisions, the abundance of water ice on the surface, and the presences of satellites in the KBO population.

6. DISCUSSION

The lack of obvious trends in color, albedo, and spectral characteristics suggests that multiple coloring agents are present in a variety of mixing ratios on KBOs. Different grain sizes of the carbon-rich materials may account for some of the observed variation in the visible gradients and albedos, but it cannot fully account for the diversity of surface properties seen in the Kuiper

belt. This may indicate inherent heterogeneity in the surface properties of the general KBO population. With the exception of very blue, icy objects, the results presented here for the NIR data do not support clear ties between the photometric colors, specific spectral types, and surface characteristics.

The modest trend in size and water ice abundance that we detected indicates that water ice may be geothermally controlled on the surfaces of KBOs. With these mechanism though, we find no evidence that suggests that these surfaces are a result of recent activity. From the minimum dynamical lifetime of the 2003 EL61 family members of approximately 1 Gyr (Ragozzine & Brown 2007), it is possible that the water ice surfaces we observe in the Kuiper belt are ancient surfaces formed when the KBOs had hotter interiors and the impact rates were higher.

At the moment, though, trends seen in our data are sufficiently tenuous that it is difficult to make any strong conclusions about the relative importance of size and collisions in determining surface properties. Our survey included nearly all the KBOs that are bright enough to easily obtain NIR spectra from large telescopes, but future spectral studies of newly discovered, bright objects, and additional albedo measurements should clarify trends seen in our data. While much remains to be learned about the overall mechanisms shaping the outer solar system bodies, we find that a comparative approach to examining spectra provides a powerful additional tool for understanding these processes.

This research is funded by the California Institute of Technology and is also supported by the NASA Planetary Astronomy program. Data presented herein were obtained at the W. M. Keck Observatory, which is operated as a scientific partnership among the California Institute of Technology, the University of California, and the National Aeronautics and Space Administration. The observatory was made possible by the generous financial support of the W. M. Keck Foundation. The authors thank Darin Ragozzine, Deanne Rogers, Timothy Glotch, and Oded Aharonson for their helpful discussions regarding this paper. We also thank Antonin Bouchez and Megan Scwamb for their help during observations.

REFERENCES

Altenhoff, W. J., Bertoldi, F., & Menten, K. M. 2004, A&A, 415, 771
Barucci, M. A., Belskaya, I. N., Fulchignoni, M., & Birlan, M. 2005, AJ, 130, 1291
Barucci, M. A., Brown, M. E., Emery, J. P., & Merlin, F. 2007, in The Solar System Beyond Neptune, ed. M. A. Barucci et al. (Tucson, AZ: Univ. Arizona Press) in press
Barucci, M. A., de Bergh, C., Cuby, J.-G., Le, Bras A., Schmitt, B., & Romon, J. 2000, A&A, 357, L53
Barucci, M. A., Merlin, F., Dotto, E., Doressoundiram, A., & de Bergh, C. 2006, A&A, 455, 725
Bauer, J. M., Meech, K. J., Fernández, Y. R., Farnham, T. L., & Roush, T. L. 2002, PASP, 114, 1309
Bevington, P. R, & Robinson, D. K. 1993, Data Reduction and Error Analysis (New York: McGraw-Hill)
Boehnhardt, H., Bagnulo, S., Muinonen, K., Barucci, M. A., Kolokolova, L., Dotto, E., & Tozzi, G. P. 2004, A&A, 415, L21
Brown, M. E. 2000, AJ, 119, 977
Brown, M. E., Barkume, K. M., Blake, G. A., Schaller, E. L., Rabinowitz, D. L., Roe, H. G., & Trujillo, C. A. 2007a, AJ, 133, 284
Brown, M. E., Barkume, K. M., Ragozzine, D., & Schaller, E. L. 2007b, Nature, 446, 294
Brown, M. E., Blake, G. A., & Kessler, J. E. 2000, ApJ, 543, L163
Brown, M. E., & Calvin, W. M. 2000, Science, 287, 107
Brown, M. E., & Koresko, C. C. 1998, ApJ, 505, L65
Brown, M. E., & Trujillo, C. A. 2004, AJ, 127, 2413
Brown, M. E., Trujillo, C. A., & Rabinowitz, D. L. 2005, ApJ, 635, L97
Clark, R. N., et al. 2005, Nature, 435, 66
Cruikshank, D. P., et al. 1998, Icarus, 135, 389
de Bergh, C., et al. 2004, A&A, 416, 791
Doressoundiram, A., Barucci, M. A., Tozzi, G. P., Poulet, F., Boehnhardt, H., de Bergh, C., & Peixinho, N. 2005a, P&SS, 53, 1501
Doressoundiram, A., Peixinho, N., Doucet, C., Mousis, O., Barucci, M. A., Petit, J. M., & Veillet, C. 2005b, Icarus, 174, 90
Doressoundiram, A., Tozzi, G. P., Barucci, M. A., Boehnhardt, H., Fornasier, S., & Romon, J. 2003, AJ, 125, 2721
Dotto, E., Barucci, M. A., Boehnhardt, H., Romon, J., Doressoundiram, A., Peixinho, N., de Bergh, C., & Lazzarin, M. 2003a, Icarus, 162, 408
Dotto, E., Barucci, M. A., Leyrat, C., Romon, J., de Bergh, C., & Licandro, J. 2003, Icarus, 164, 122
Fornasier, S., et al. 2004, A&A, 421, 353
Foster, M. J., Green, S. F., McBride, N., & Davies, J. K. 1999, Icarus, 141, 408
Grundy, W. M., Noll, K. S., & Stephens, D. C. 2005, Icarus, 176, 184
Grundy, W. M., & Schmitt, B. 1998, J. Geophys. Res., 103, 25809
Grundy, W. M., Young, L. A., Spencer, J. R., Johnson, R. E., Young, E. F., & Buie, M. W. 2006, Icarus, 184, 543
Hainaut, O. R., & Delsanti, A. C. 2002, A&A, 389, 641
Hansen, G. B., & McCord, T. B. 2004, J. Geophys. Res. (Planets), 109, 1012
Hapke, 1993, Theory of Reflectance and Emittance Spectroscopy (Cambridge, MA: Cambridge Univ. Press)
Jewitt, D. C., & Luu, J. X. 2001, AJ, 122, 2099
Jewitt, D. C., & Luu, J. 2004, Nature, 432, 731
Kouchi, A., & Kuroda, T. 1990, Nature, 344, 134
Licandro, J., di Fabrizio, L., Pinilla-Alonso, N., de León, J., & Oliva, E. 2006, A&A, 457, 329
Licandro, J., Ghinassi, F., & Testi, L. 2002, A&A, 388, L9
Licandro, J., Oliva, E., & Di Martino, M. 2001, A&A, 373, L29
Licandro, J., Pinilla-Alonso, N., Pedani, M., Oliva, E., Tozzi, G. P., & Grundy, W. M. 2006, A&A, 445, L35
Luu, J., & Jewitt, D. 1996, AJ, 112, 2310
Luu, J. X., Jewitt, D. C., & Trujillo, C. 2000, ApJ, 531, L151
Matthews, K., & Soifer, B. T. 1994, ExA, 3, 77
Merlin, F., Barucci, M. A., Dotto, E., de Bergh, C., & Lo Curto, G. 2005, A&A, 444, 977
Merlin, F., Guilbert, A., Dumas, C., Barucci, M. A., de Bergh, C., & Vernazza, P. 2007, A&A, 466, 1185
Moore, M. H., Donn, B., Khanna, R., & A'Hearn, M. F. 1983, Icarus, 54, 388
Noll, K. S., Grundy, W. M., Chiang, E. I., Margot, J.-L., & Kern, S. D. 2007, in The Solar System Beyond Neptune, ed. M. A. Barucci et al. (Tucson, AZ: Univ. Arizona Press) in press
Ortiz, J. L., et al. 2004, A&A, 420, 383
Pinilla-Alonso, N., Licandro, J., Gil-Hutton, R., & Brunetto, R. 2007, A&A, 468, L25
Rabinowitz, D. L., Barkume, K., Brown, M. E., Roe, H., Schwartz, M., Tourtellotte, S., & Trujillo, C. 2006, ApJ, 639, 1238
Rabinowitz, D. L., Schaefer, B. E., & Tourtellotte, S. W. 2007, AJ, 133, 26
Ragozzine, D., & Brown, M. E. 2007, AJ, 134, 6
Romon-Martin, J., Barucci, M. A., de Bergh, C., Doressoundiram, A., Peixinho, N., & Poulet, F. 2002, Icarus, 160, 59
Romon-Martin, J., Delahodde, C., Barucci, M. A., de Bergh, C., & Peixinho, N. 2003, A&A, 400, 369
Schaller, E. L., & Brown, M. E. 2007, ApJ, 659, L61
Stansberry, J., Grundy, W., Brown, M., Cruikshank, D., Spencer, J., Trilling, D., & Margot, J.-L. 2007, in The Solar System Beyond Neptune, ed. M. A. Barucci et al. (Tucson, AZ: Univ. Arizona Press) in press
Strazzulla, G., Leto, G., Baratta, G. A., & Spinella, F. 1991, J. Geophys. Res., 96, 17547
Trujillo, C. A., Brown, M. E., Barkume, K. M., Schaller, E. L., & Rabinowitz, D. L. 2007, ApJ, 655, 1172
Trujillo, C. A., Brown, M. E., Rabinowitz, D. L., & Geballe, T. R. 2005, ApJ, 627, 1057